Geophysical Research Letters

RESEARCH LETTER
10.1029/2019GL085992

**Key Points:**
- Phytoplankton onset is detected from in situ high-resolution multisensor data gathered by one mooring and two Biogeochemical Argo floats
- The bloom starts approximately 2 months after the net heat flux becomes positive, during an abrupt shoaling event of the mixing layer
- The bloom starts only after a decrease in the depth over which winds actively mix the upper ocean leading to a decrease of the turbulence

**Supporting Information:**
- Supporting Information S1

**Correspondence to:**
V. Pellichero,
violaine.pellichero@gmail.com

**Citation:**
Pellichero, V., Boutin, J., Claustre, H., Merlivat, L., Sallée, J.-B., & Blain, S. (2020). Relaxation of wind stress drives the abrupt onset of biological carbon uptake in the Kerguelen bloom: A multisensor approach. *Geophysical Research Letters*, *47*, e2019GL085992. https://doi.org/10.1029/2019GL085992

Received 24 OCT 2019
Accepted 5 APR 2020
Accepted article online 17 APR 2020



# Relaxation of Wind Stress Drives the Abrupt Onset of Biological Carbon Uptake in the Kerguelen Bloom: A Multisensor Approach

**Violaine Pellichero[1], Jacqueline Boutin[1], Hervé Claustre[2], Liliane Merlivat[1], Jean-Baptiste Sallée[1], and Stéphane Blain[3]**

[1]CNRS, IRD, MNHN, UMR 7159, Laboratoire d'Océanographie et du Climat: Expérimentations et Approches Numériques, LOCEAN-IPSL, Sorbonne Université, Paris, France, [2]CNRS, UMR 7093, Laboratoire d'Océanographie de Villefranche, LOV, Sorbonne Université, Paris, France, [3]CNRS, UMR 7621, Laboratoire d'Océanographie MICrobienne, LOMIC, Sorbonne Université, Paris, France

**Abstract** We deployed sensors for physical and biogeochemical measurements on one Eulerian mooring and two Lagrangian biogeochemical Argo floats on the Kerguelen Plateau. High temporal and vertical resolution measurements revealed an abrupt shoaling of both the mixed-layer depth and mixing-layer depth. The sudden stratification was concomitant with the start of significant biological activity detected by chlorophyll-a accumulation, oxygen oversaturation, and dissolved inorganic carbon drawdown. The net community production computed in the mixing-layer during the onset period of 9 days was $119 \pm 7$ mmol·m$^{-2}$·day$^{-1}$. While it is generally admitted that bloom initiation is mostly driven by the onset of positive heat fluxes, our results suggest that this is not a sufficient condition. Here we report that the decrease in the depth over which wind mixes the upper layer drives the initiation of the bloom. These results suggest that future atmospheric changes in Southern Ocean could impact the phenology of the blooms.

**Plain Language Summary** The region of the Kerguelen Plateau is well known as a naturally iron-fertilized region, and it supports a productive marine ecosystem. In the present study, we investigate the evolution of the biogeochemical and physical conditions during the 2016 phytoplankton bloom event near the Kerguelen Plateau. We use a unique combination of moored instruments and profiling floats in order to follow the phytoplankton evolution at vertical, spatial, and temporal scales and to understand the main physical drivers supporting such an abrupt bloom initiation that occurs only over a 9-day period. The large phytoplankton bloom develops during a major shallowing event bringing in few days the mixed-layer depth from its typical winter value to its typical summer value. This abrupt stratification of the water column is driven by a decline of the wind stress. These results have important implications considering that the wind regimes are predicted to intensify in the future in the Southern Ocean.

## 1. Introduction

More than 30 years ago, the Southern Ocean (SO) has been classified as a high-nutrient low-chlorophyll region (Minas et al., 1986). During the following decades, convincing arguments have been provided to explain that low-nutrient utilization and therefore inefficient biological carbon pump in this ocean resulted primarily from iron limitation of photosynthetic microorganisms (Blain et al., 2007; Boyd et al., 2000; Martin, 1990). However, the increasing number of observations coming from both field studies and autonomous sensors embarked on various in situ or satellite vectors revealed that the "low-chlorophyll" historical view of the SO embedded more complex spatial and temporal patterns. From the examination of seasonal cycles of surface chlorophyll, a patchy regionalization emerged, which could not be firmly linked to environmental properties of the usual provinces of the SO (Thomalla et al., 2011). When the mixed-layer depth (MLD) was taken into account, three different types of SO blooms were defined, which coincide with distinct dynamical regions (Sallée et al., 2015). More recently, Ardyna et al. (2017) combined in situ measurements, satellite observations, and model outputs to suggest that environmental controls delineate seven different bioregions with respect to phytoplankton biomass and phenology. All these studies have made an extensive use of chlorophyll-a concentration (Chla), both at the surface and in the water column, as a proxy of phytoplankton biomass.

The phenology of phytoplankton blooms has received considerable attention because it depends on forcing parameters that might be altered by climate change (e.g., heat flux, wind stress, and freshening) and also because it is strongly linked to essential marine ecosystem services (e.g., resources or carbon sink) (Jones et al., 2016). Various conceptual frameworks have been proposed to explain the onset of the spring blooms (Behrenfeld, 2010; Brody & Lozier, 2015; Chiswell, 2011; Mignot et al., 2018; Sverdrup, 1953; Taylor & Ferrari, 2011). However, other facets of phytoplankton bloom, such as the dynamics of biological $CO_2$ uptake, have received much less attention.

This is a very challenging task if high-resolution or long-term measurements are targeted. In the SO, different strategies have been used. Underway measurements of partial pressure of $CO_2$ ($pCO_2$) in the surface waters (Bakker et al., 2015) largely contributed to the assessment of Southern Ocean $CO_2$ sink and its variability (Landschützer et al., 2015). Lagrangian surface drifters (CARIOCA buoy) equipped with $pCO_2$, fluorescence, or $O_2$ sensors revealed the high spatial and temporal variability of the carbon fluxes in response to physical and biological changes (Boutin et al., 2008; Resplandy et al., 2014). The net community production (NCP), that can be used cautiously as a proxy of the carbon export, was also derived from the CARIOCA measurements (Merlivat et al., 2015). Provided appropriate alkalinity (Alk) parametrization, Biogeochemical-Argo profiling floats (hereafter BGC-Argo) equipped with pH and $O_2$ sensors have recently been proposed to estimate $pCO_2$ in various provinces on the SO over full seasonal cycles (Gray et al., 2018). A large spatial coverage of NCP in the SO was reported using underway ($O_2$/Ar) measurements (Cassar et al., 2007). Eulerian approaches to the estimate of $pCO_2$ in the SO have also been pioneered by instrumented moorings deployed in the sub-Antarctic zone of Tasmania from which temporal description and quantification of different carbon fluxes were successfully derived (Shadwick et al., 2015; Weeding & Trull, 2014).

In our study conducted in the naturally iron-fertilized region of Kerguelen (Blain et al., 2007), south of the polar front, we take advantage of the in situ high-resolution multisensor data set gathered by one mooring and two BGC-Argo floats to look carefully at biological signatures during the early stage of the bloom from a multiple parameter perspective. In addition to changes in Chla, temporal variations in dissolved oxygen ($O_2$) and dissolved inorganic carbon (DIC) provide new insights on the short-term variability of carbon stocks and fluxes. We assess bloom initiation dynamics in relation to heat flux and wind stress changes.

## 2. Data Sources and Processing

During the Southern Ocean and Climate—Field Studies with Innovative Tools (SOCLIM) cruise (DOI: 10.17600/16003300), an instrumented mooring and two profiling BGC-Argo floats were deployed in spring 2016 on the central Kerguelen Plateau. The atmospheric context at the time of measurements is documented using atmospheric reanalysis. The climatological and synoptic context of our area of interest is described using a combination of satellite and in situ observations. Full details of all materials and methods are provided in the Acknowledgment section and supporting information. Here we provide a brief outline.

### 2.1. SOCLIM Mooring

One anchored mooring was deployed from 18 October 2016 to 6 April 2017 in the central part of the Kerguelen Plateau, at 50°37′135°S and 072°06′179°E (Figure 1), where the waters are naturally enriched in iron leading to enhanced phytoplankton bloom development (Blain et al., 2007, 2008; Jouandet et al., 2008). This mooring was equipped with a package of sensors located at 42-m depth. A Sea-Bird SBE-16 sensor measured hourly conductivity and temperature. An Anderaa optode, with post cruise calibration by the manufacturer, provided hourly $O_2$ measurements. A Carioca sensor, calibrated using DIC and Alk profiles at the mooring site in October 2016 and January 2017 (OISO cruise), according to the protocols described in Merlivat et al. (2017), provided hourly measurements of $pCO_2$.

The mooring line between 42 and 300 m was equipped with 10 Sea-Bird SBE-37 (conductivity, temperature, and pressure), and 22 Sea-Bird SBE-56 sensors (temperature) were also deployed between the SBE-37 loggers. Altogether, these sensors provided profiles between 42 and 300 m with a temporal resolution of 30 min and a vertical resolution of 30 and 5 m for salinity and temperature, respectively.

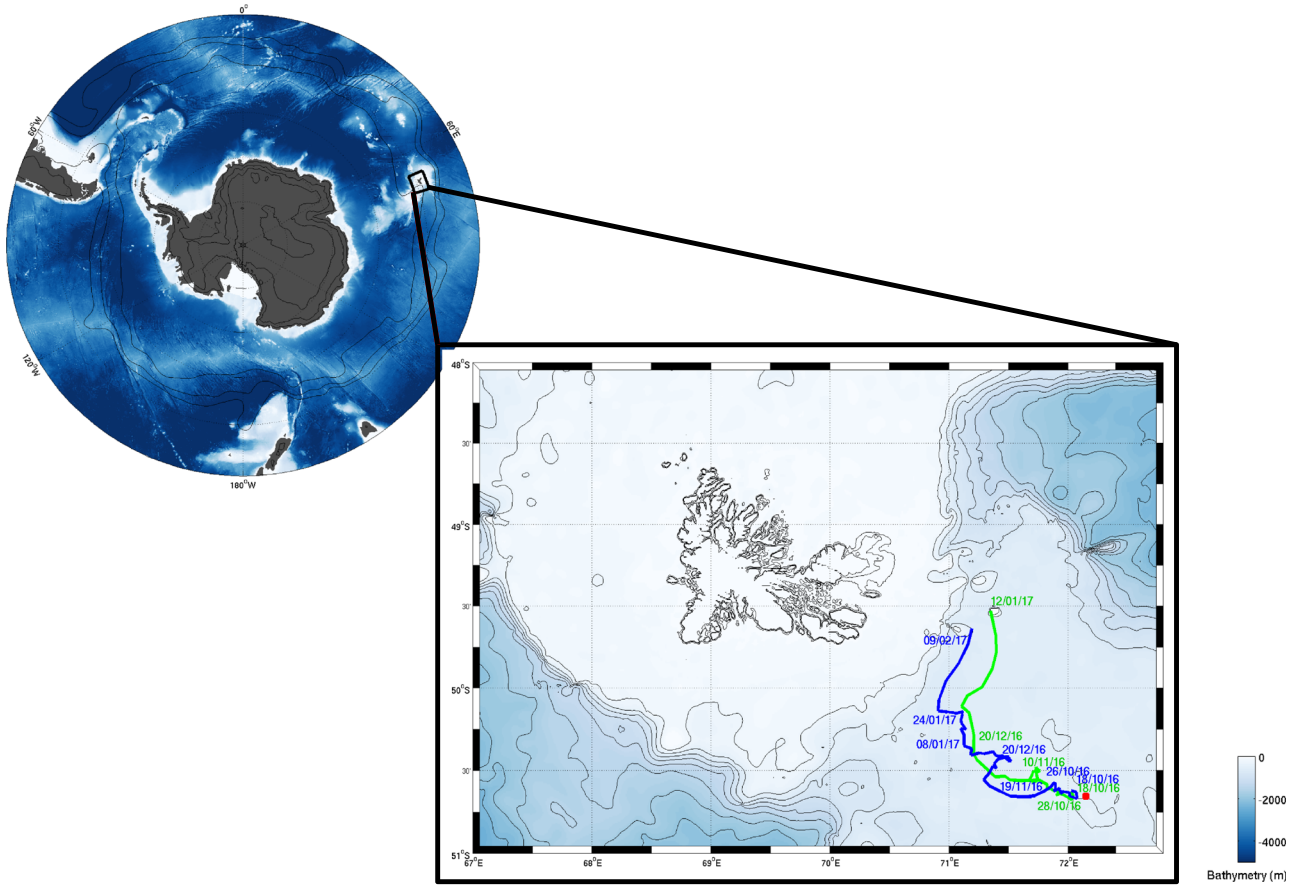


**Figure 1.** Map of the Southern Ocean, showing major topography and a zoom on the studied area near Kerguelen. The mooring is located near Kerguelen (red point); bathymetry contours spaced every 500 m are in black. The two BGC-Argo float trajectories within 100 km from the mooring are in blue (WMO 6902736) and green (WMO 6902737) from 18 October 2016 to 9 February and 1 January 2017, respectively.

### 2.2. BGC-Argo Floats

Two BGC-Argo profilings (WMO 6902737 and WMO 6902736) were also deployed on 18 October 2016, near the mooring location (Figure 1). Both floats sampled the water column between 300 m and the surface with a vertical resolution of 1 m, once a day during 18 days (18 October to 5 November 2016). Afterward, the temporal resolution was relaxed to one profile every 2 days during 114 days (5 November 2016 to 27 February 2017) and one profile every 4 days from 27 February 2017 to the end of batteries (8 April 2018 for WMO 6902736 and 12 June 2018 for WMO 6902737). For the purpose of this study, we only display data over a 2-month time period between 18 October and 20 December 2016.

Both BGC-Argo floats were equipped with a SBE41CP Seabird CTD, a WET Labs ECO sensor including a Chla fluorometer (excitation at 470 nm and emission at 695 nm), and an OC4 radiometric sensor that measures the photosynthetically available radiation (PAR). The measurements were quality controlled according to internationally agreed procedures (Roesler et al., 2017; Schmechtig & Thierry, 2016). The instantaneous profile of $PAR_i$ was first converted into a daily average profile as described in Mignot et al. (2014). Subsequently, the daily average profile was further averaged over the mixed layer and mixing layer (respectively, $PAR_{MLD}$ and $PAR_{MixLD}$). Additionally, the euphotic zone depth, Zeu (m), was computed as the depth where PAR reaches 1% of its surface value.

### 2.3. Atmospheric Parameters

Net air-sea heat flux, 10-m wind speed, and wind stress are estimated at the mooring location for the period 2016–2017 from four different products (Figures 2c and 2d): the Japanese 55-year reanalysis, NCEP1 reanalysis, ERA5 reanalysis, and a product derived from satellite observations OAFlux + CERES.

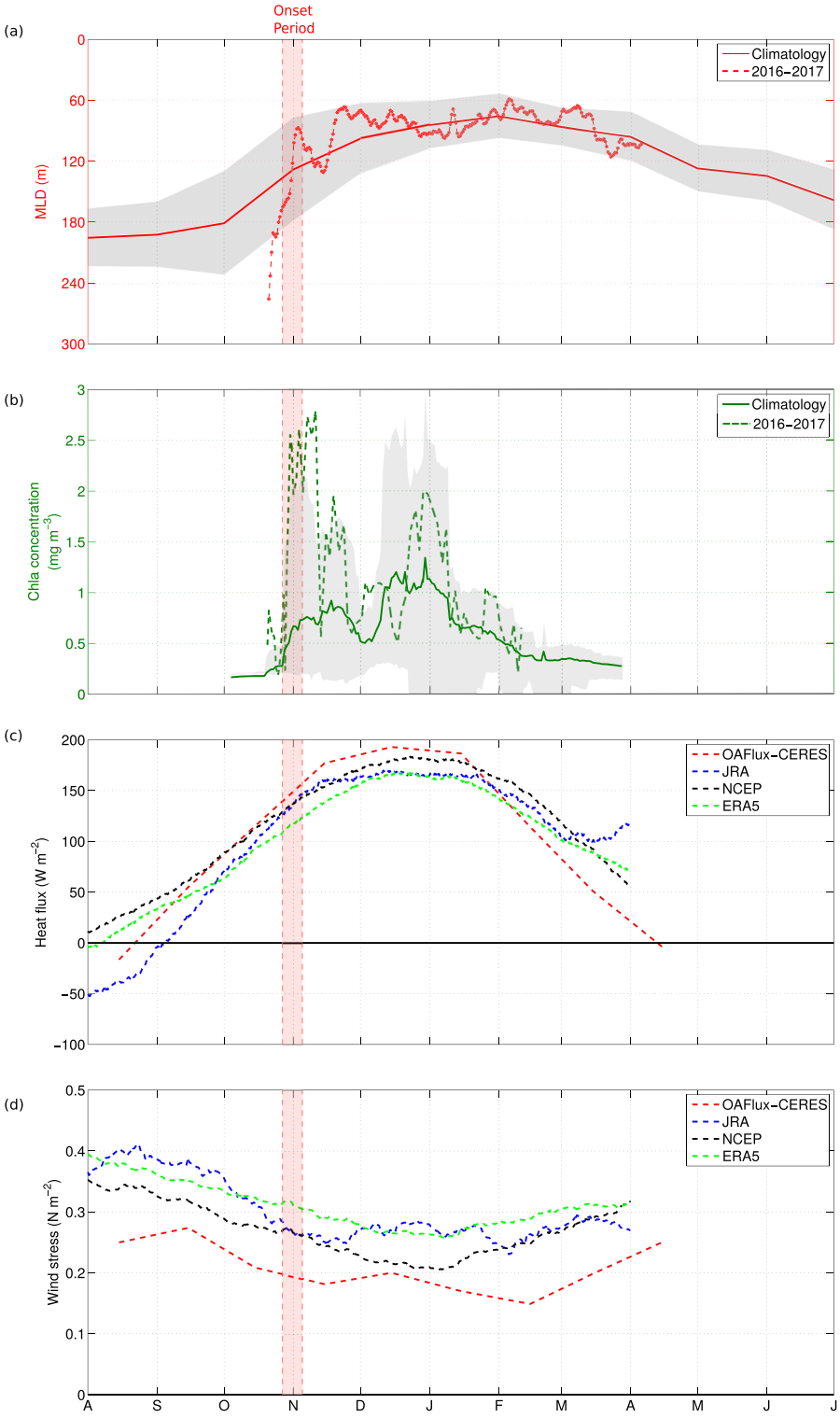


**Figure 2.** 2016–2017 observations (a and b) and reanalysis (c and d) at the mooring location and comparison to climatology (a and b). (a) MLD (m) from the mooring (dashed line) and climatology (plain line) at the mooring location as derived by Pellichero et al. (2017)—standard deviation in gray. (b) Chla averaged over 10-m depth as recorded by WMO 6902737 BGC float (dashed line) and satellite climatology at the mooring location (plain line; standard deviation in gray). (c) Net heat flux for the period 2016–2017 (W·m$^{-2}$) at the mooring site from JRA-55 reanalysis (blue), ERA5 (green), NCEP1 (black), and a product derived from satellite observations OAFlux + CERES (red). (d) Wind stress for the period 2016–2017 (N·m$^{-2}$) at the mooring site from JRA-55 reanalysis (blue), ERA5 (green), NCEP (black), and OAFlux (red). On each panel, the red shading highlights the period of interest in this study, corresponding to the onset of the bloom period as defined in section 3.3.

The air-sea $CO_2$ flux is derived using the 10-m wind speed at the mooring location from the Japanese 55-year reanalysis for the period 2016–2017 and atmospheric $pCO_2$ recorded at Crozet Island.

### 2.4. Estimation of the MLD and Mixing-Layer Depth

The properties and vertical extent of the mixed layer are central metrics for understanding phytoplankton dynamics (Sverdrup, 1953). The MLD refers to the depth of vertically homogeneous profile of temperature, salinity, and density. MLD is computed from both the BGC-Argo floats and the mooring profiles. For the mooring, the temperature profiles have a higher vertical resolution (5 m) than the density profile (30 m). Consequently, MLD is estimated from a temperature-based criterion (temperature difference threshold from the surface temperature of $\Delta T = 0.2$ °C) (de Boyer Montégut et al., 2004; Holte & Talley, 2009; Pellichero et al., 2017; Sallée et al., 2006). One important limitation is we do not have access to the surface temperature from the mooring data set. We therefore assume the surface temperature to be equal to the shallowest available temperature at 42 m and apply the temperature threshold from there. The MLD from the profiling floats computed both with and without assuming well-mixed temperature within the upper 42 m is very close; however, a few particular events of shallow mixed layer are missed (Supporting Information S1). In addition, using a temperature threshold rather than a density threshold gives similar results on MLD derived from profiling float data, which provides us confidence in our MLD detection methods (Supporting Information S1).

While the MLD is an important parameter, contemporary studies have also highlighted the significance of the "mixing layer" to study the phenology of the phytoplankton bloom (Brody & Lozier, 2015; Taylor & Ferrari, 2011). The mixing layer can be defined as the depth in which turbulence is fully and actively driven by surface forcing (Stevens et al., 2011). We estimated the mixing-layer depth as the Ozmidov length from the mooring time series and JRA-55 wind stress. Wind stress from different reanalysis is also introduced in Supporting Information S2 as well as all details of calculation of the mixing-layer depth.

### 2.5. Carbon Fluxes and NCP

The period of interest highlighted in this study, namely, the "onset period," which corresponds to a rapid modification of the biogeochemical parameters, is defined from the multisensor analysis of the DIC, oxygen, and Chla that attests the start of a strong biological activity between 27 October and 5 November 2016. This bloom is indicated by the red shading on all the figures.

DIC concentration was calculated using CARIOCA $pCO_2$, temperature, and alkalinity derived from salinity with a regional relationship as in Merlivat et al. (2015). Based on measurements of Chla and density profiles in the upper layer of the North Atlantic Ocean, Lacour et al. (2019) have shown that at the beginning of the spring, the productive layer is shallower than the mixed layer. This result is consistent with our BGC-Argo float observations (Figure 3d and Supporting Information S3) showing higher values of the Chla above the base of the mixing layer, which is shallower than the mixed layer. Hence, in the following, we consider that the NCP occurs in the mixing layer only and that phytoplankton cells are homogeneously distributed by the mixing in that layer so that the biological carbon uptake is also vertically homogeneous. The NCP, over a few days' time interval, is derived assuming that (1) DIC at 42-m depth is within the mixing layer and (2) horizontal advection and (3) vertical mixing are both negligible. These hypotheses are supported during the onset period between 27 October and 5 November 2016, by several evidences. First, the 42-m sensors are within the mixinglayer estimates (Figure 3a), except for a short period around 3 November 2016 (indicated as dotted line in Figure 3a). However, taking this short period into account or not does not affect our NCP estimates. Second, the Chla recorded by the mooring and by the Lagrangian floats qualitatively varies similarly (Supporting Information S4), and finally, the mooring temperature regularly increases as expected in a near surface layer isolated from the subsurface layers (Figure 3c). We neglect the eddy diffusion term because the DIC gradient at the basis of the mixing layer is expected to be much smaller than the one at the basis of the mixed layer. Therefore, NCP is estimated from the slope in time of DIC integrated over the mixing-layer depth ($DIC_{int}$) corrected from the air-sea flux contribution:

$$NCP = \left(\frac{\Delta DIC_{int}}{\Delta t}\right)_{bio} = \left(\frac{\Delta DIC_{int}}{\Delta t}\right)_{meas} - k \times s \times (pCO_{2atm} - pCO_{2sw}) \quad (1)$$

The first term at the right-hand side of equation 1, "meas," corresponds to the measured temporal change of $DIC_{int}$ derived from $pCO_2$ observations, and the second term corresponds to DIC change due to air-sea $CO_2$

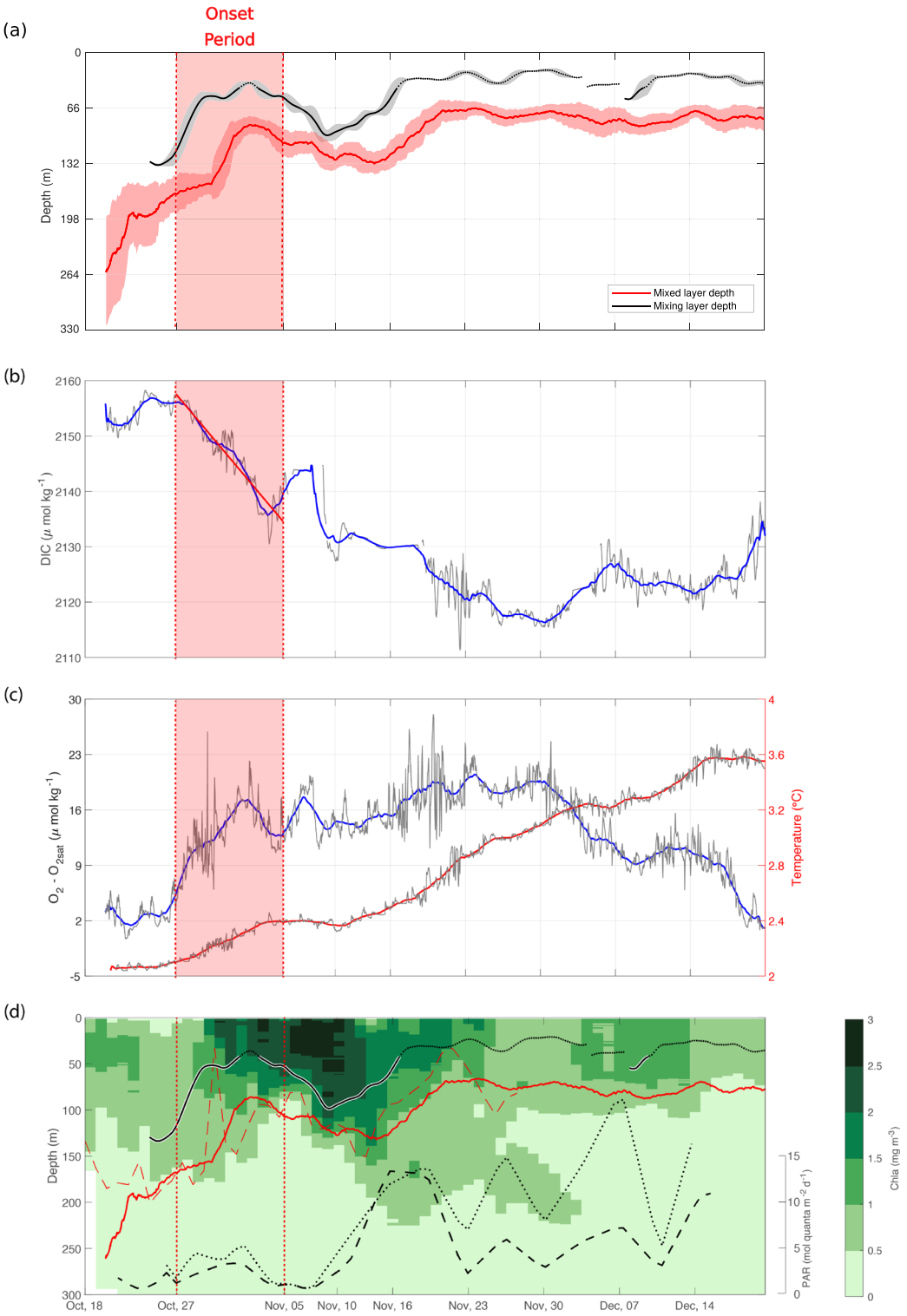


**Figure 3.** Multiparameter detection of biological activity rise. (a) MLD and mixing layer (respectively, red and black) computed at the mooring site, with 24-hr running standard deviation is shown as shading around the curves. The dotted parts of the black line correspond to period where the mixing layer is above 42 m. (b) DIC time series (blue) and linear regression from 27 October to 5 November 2016 (red line). (c) Time series of the oxygen oversaturation (blue) and temperature records by the mooring at 42 m (red). (b and c) Data at 1-hr resolution (gray) and averaged with a 2-day running mean (color). (d) Vertical section of Chla (WMO 6902737 BGC-Argo float); MLD and mixing layer computed at the mooring site are shown as plain red and black lines, respectively, and MLD from the float time series is shown as red dashed line for comparison; $PAR_{MLD}$ and $PAR_{MixLD}$ are shown as black dashed and dotted lines, respectively. On all panels, the onset period of the bloom (27 October to 5 November 2016) is shown as the two vertical red dashed lines as well as red shading for panels (a)–(c).

flux (further details in Supporting Information S5 and in other studies; Dickson & Millero, 1987; Mehrbach et al., 1973; Park et al., 2008; Wanninkhof, 2014).

## 3. Results and Discussion

### 3.1. Temporal Variability of Physical and Biological Parameters at the Mooring Site

The climatological seasonal cycle of the MLD around the mooring site (Figure 2a) varies from 180 m in winter (J-A-S) to 80 m in summer (J-F-M). The mooring 2016–2017 MLD is very close to the climatological values except during spring (O-N) where the mooring records faster and stronger restratification as well as deeper MLD than usual in late winter. The MLD rapidly shallowed from about 250 m at the end of October 2016 to ~70–80 m, 10 days later. During the same period, the BGC-Argo WMO 6902737 float recorded a strong increase of Chla (0.5 to 2.5 $mg{\cdot}m^{-3}$; Figure 2b). Similar temporal changes of Chla were also observed with the mooring and with the second BGC-Argo float (Supporting Information S4). A second bloom was also detected later in the season, also consistent with the climatology (see Supporting Information S6 for more details on the Chla climatology). In this paper we only focus on the first bloom as during the second bloom, the BGC-Argo floats were already 100 km away from the mooring and this later bloom occurred at a date when additional vertical DIC fluxes (i.e., entrainment) took place at the base of the MLD making equation 1 less reliable.

Heat fluxes and wind speed are two major drivers of the turbulence in the MLD (Belcher et al., 2012; Dong et al., 2008; Kraus & Turner, 1967; Sallée et al., 2010). The 2016–2017 seasonal variability of the net heat fluxes is overall consistent across four different reanalysis products (Figure 2c), despite few significant differences between them (e.g., period where the heat fluxes switch from negative to positive). The heat flux minimized in winter with a mean value of $-50$ $W{\cdot}m^{-2}$ (JRA-55) and maximized at the end of spring/early summer with a mean value around 160 $W{\cdot}m^{-2}$. When heat flux becomes null or slightly positive (in 2016, early August for NCEP and ERA5, mid-August for OAFlux, and early September for JRA-55), it acts as a stabilizer transferring heat from the atmosphere into the ocean and then stratifying the water column.

Similarly, the wind stress estimated from the same four reanalysis products (Figure 2d) is consistent for the 2016–2017 season with a climatological cycle that maximizes in winter with values ranging from 0.28 $N{\cdot}m^{-2}$ (OAFlux) to 0.4 $N{\cdot}m^{-2}$ (JRA-55) and gradually decreases over the season until reaching its minimum value at the end of spring/early summer.

### 3.2. Atmospheric Drivers of Rapid Change in Surface Layer

While the 2016–2017 environmental seasonal cycle at the mooring site, as described by MLD and Chla, appears consistent with the climatological mean seasonal cycle, the 2016–2017 period is marked by abrupt changes at the end of October, characterized by rapid shallowing of the MLD, and marked increase of Chla between 27 October and 5 November 2016 (Figures 2a and 2b). Zooming on the MLD time series, it appears however that the rapid increase in Chla leads the marked shallowing of the MLD by few days (Figure 3a). Some studies have argued that Chla increase would precede shallowing of the MLD, because active mixing in the MLD would be reduced days before the stratification increase reducing the MLD (e.g., Brody & Lozier, 2014; Taylor & Ferrari, 2011). Many studies have used air-sea heat flux as a proxy to define when the active mixing in the MLD is stopped at the end of winter (e.g., Taylor & Ferrari, 2011), assuming that active mixing stops when air-sea heat flux switches from negative to positive values (which warm the ocean surface, thus stratifying the water column).

In the present study, the four heat flux products are already positive several weeks before MLD and Chla rapid increase in late October (Figure 2c). Therefore, while positive heat fluxes may be a necessary condition of reduced mixing activating Chla increase, this is not sufficient to initiate biomass accumulation. Interestingly, winds are at their annual maximum strengths in August and September, gradually reducing until late October, suggesting that even if the heat fluxes are stratifying, the wind could be strong enough to maintain enough turbulence into the surface and keep the mixed layer at depth, hence preventing bloom onset. This is in line with Brody and Lozier (2015) analyses suggesting that decreases in the depth of active mixing are a result of the transition from buoyancy-driven to wind-driven mixing and control the timing of the spring bloom. Here we focus on reduced turbulence rather than change of advection (lateral or vertical) that could potentially impact the stratification, because our observations show that the mixed layer is

actually destratified (i.e., deep MLD), when the Chla increase starts. If that Chla increase would be supported by change of large-scale advection changing the stratification (e.g., change in wind stress curl), we would observe a fingerprint in the density field, that is, observe a change of MLD. Similarly, at short temporal scales and small spatial scales as studied here, submesoscale dynamics within the mixed layer have been reported to play a role in restratifying the mixed layer (Lévy et al., 2018; Siegelman et al., 2020). However, if submesoscale processes would be the main cause of the stratification event, it would have a fingerprint on the density field, hence would be associated with a shallowing of the MLD, which is not observed on 27 October. Submesoscale might be active and act to restratify after that period when turbulence relaxes (even though some analyses suggest that it might be a weak effect in our region; Rosso et al., 2016). Instead, we hypothesize here that the density field remains unchanged but the local turbulence reduces, allowing a Chla increase (e.g., Brody & Lozier, 2015; Taylor & Ferrari, 2011).

This hypothesis is confirmed through the analysis of temporal variation of the Ozmidov length (Figure 3a, Supporting Information S2). This scale gives a measure of the typical depth over which mixing occurs under stable stratification and at a given turbulence rate, here estimated to come from wind stress (Brody & Lozier, 2015; Denman & Gargett, 1983; Riley & Lelong, 2000). Using this scale to quantify the balance between both wind stress effect and buoyancy forcing effect over the ocean surface, it appears that despite restratifying forces from air-sea heat fluxes, the wind actively mixes the surface layer up to 130 m before 27 October and rapidly switches to mix a much shallower layer of ~50 m, after 27 October (Figure 3a). Our results therefore suggest that a shoaling of the mixing layer (i.e., decrease of the mixing) precedes a shoaling of the MLD and corresponds to the onset of the bloom. These observations suggest that variations in the wind stress first modulate the variations of the mixing layer and second of the MLD, consistent with wind-induced mechanical mixing (Carranza & Gille, 2015; Carranza et al., 2018; Dong et al., 2008; Gille et al., 2014; Mahadevan et al., 2010, 2012). We now investigate how this change of surface mixing translates into change of biological parameters and carbon uptake, beyond the simple fingerprint on Chla concentration.

### 3.3. Multiparameter Detection of the Rapid Bloom Onset

A large decrease of DIC (Figure 3b), a rapid increase in the $O_2$ oversaturation, and an increase of the temperature (Figure 3c) are observed at the mooring site at 42-m depth from 27 October to 5 November. These gathered parameters unambiguously attest the start of a strong biological activity on 27 October (i.e., the onset date of the phytoplanktonic bloom). The estimate of NCP integrated over the mixing layer is equal to $119 \pm 7$ mmol·m$^{-2}$·day$^{-1}$ and compares well with the average daily NCP of $99 \pm 37$ mmol·m$^{-2}$·day$^{-1}$ computed by Jouandet et al. (2008) at the same site using a seasonal DIC budget approach. It is not surprising that the present estimate is above this seasonal mean value because, at this site, the daily NCP is higher at the beginning of the season than later when high heterotrophic bacterial activity takes place (Obernosterer et al., 2008).

During this period of intense biological activity, the phytoplankton bloom develops as indicated by a large and rapid increase of the Chla (Figure 3d). Over both the entire mixing layer and MLD, the averaged Chla also increases (Supporting Information S7) but with a higher magnitude in the mixing layer. NCP derived by assuming that DIC is vertically homogeneous over the mixing layer ($119 \pm 7$ mmol·m$^{-2}$·day$^{-1}$) greatly differs from the estimate obtained by assuming that DIC is vertically homogeneous over the whole mixed layer ($212 \pm 7$ mmol·m$^{-2}$·day$^{-1}$; see Supporting Information S5). This result is in line with an overestimation of the Chla stock calculated by multiplying the surface Chla by the depth of the MLD rather than by the depth of the mixing layer in which the biology actively develops (Lacour et al., 2019).

The changes in the various parameters (DIC, $O_2$, and Chla) pinpoint to a rise of the biological activity concomitant with the rapid shallowing of the mixing layer (Figure 3) suggesting a direct link between both processes. The shallowing of the mixing layer is associated with an increase of the daily average PAR within both the mixed and mixing layers (Figure 3d) from less than 1.3 mol·quanta·m$^{-2}$·day$^{-1}$ on the 26 of October to peak at 5.2 mol·quanta·m$^{-2}$·day$^{-1}$ 2 days later. These values are in close agreement to regional average values reported for the productive zone eastward of the Kerguelen Plateau (Blain et al., 2013). Concomitantly, the euphotic zone depth, Zeu, decreases from about 60 m just before the bloom on 27 October, to a minimum of ~30 m on 2 November (not shown). These observations suggest that the

seasonal rise of the surface PAR combined with the rapid shallowing of the mixing layer increased $PAR_{MixLD}$ above the winter value and triggered the abrupt increase of the biological activity. We also note that $PAR_{MixLD}$ decreased when the mixing layer stopped shallowing and then increased again when the mixing layer shallowed (around 10 November 2016) and part of the surface biomass was exported below the mixing layer around mid-November. This temporal pattern is consistent with previous observations (Blain et al., 2013) suggesting that self-shading imposed an upper limit to the light available during the development of the bloom and had a strong influence on the maximum amount of biomass that can accumulate in the mixing layer.

## 4. Conclusion

A multiplatform investigation acquiring multidisciplinary data at the appropriate temporal resolution is used to refine a mechanistic understanding of the environmental setup required for the phytoplankton spring bloom onset on the Kerguelen Plateau. Our primary conclusion is that, while the reversal of heat fluxes from destratifying to stratifying force may be a necessary condition for spring bloom onset, it is not a sufficient one when wind is properly strong to actively mix the surface layer deep enough. The bloom described in the present study starts nearly 6 weeks after the heat flux reversal. The present study emphasizes the critical role of wind stress, which can continue to maintain phytoplankton biomass at its winter level. It is only when wind stress diminishes to a given threshold that turbulence becomes sufficiently alleviated and the mixing layer reduced for the bloom to start, thanks to a sufficient light availability within the reduced mixing layer. While such a mechanism was already suggested at play for bloom initiation in the North Atlantic by Brody and Lozier (2015), it is the first time that it is documented in the SO, together with the associated DIC decrease. In such a configuration, our data highlight the abrupt DIC decrease as a mirror of biomass increase. We further suggest that such DIC changes might represent alternate metrics for bloom onset characterization in terms of timing and magnitude.

More generally, our results confirm that wind regime is an important driver of the phenology of the bloom of the central Kerguelen Plateau as previously reported in the SO (Carranza & Gille, 2015; Carranza et al., 2018; Gille et al., 2014). These observations have significant implications for the understanding of the variability of blooms. At the interannual time scale, variability in wind stress could likely be responsible for the observed variability in the bloom timing. Furthermore, the wind regimes are predicted to change in the future as a result of climate change, with potential complex counterbalanced effect of increased stability of the water column due to surface-intensified warming and increased wind stress (Bracegirdle et al., 2013). The Kerguelen bloom sustains a unique ecosystem, which includes important marine resources.

**Acknowledgments**
We thank the captains and the crew of the R/V Marion Dufresne for their support during the cruise. We thank people from DT-INSU, Institut Polaire Paul Emile Victor (IPEV), LOCEAN/DITM, and LOV teams for the technical support. This work is part of the project SOCLIM supported by the Climate Initiative of the foundation BNP Paribas, the French research program LEFE-CYBER of INSU-CNRS, IPEV, Sorbonne Université, and the Flotte Océanographique Française. It was also supported by the EU FP7 Carbochange project (Grant Agreement 264879) and by the remOcean project funded by the European Research Council (Grant Agreement 246777). Data supporting the conclusions are freely available at http://doi.org/10.17882/42182 (Argo data) and at https://doi.org/10.17882/71768 (mooring data). Air-sea data set is freely available at http://jra.kishou.go.jp (JRA-55), https://www.esrl.noaa.gov/psd/data/gridded/data.ncep.reanalysis.html (NCEP1), https://www.ecmwf.int (ERA5), and http://oaflux.whoi.edu/data.html (OAFlux + CERES). The marine mammal data are freely available by the International MEOP Consortium and the national programs that contribute to it (http://www.meop.net). J.-B. S. was supported by the European Research Council under the European Union's Horizon 2020 research and innovation program (Grant Agreement 637770). Catherine Schmechtig is acknowledged for managing the SOCLIM database. Marin Cornec is acknowledged for computing metrics related to light measurements on the floats. V. P. is supported by the Australian Research Council Discovery Grant 160103130 and through funding from the Earth Systems and Climate Change Hub of the Australian government's National Environmental Science Program.

## References

Ardyna, M., Claustre, H., Sallée, J. B., D'Ovidio, F., Gentili, B., Van Dijken, G., et al. (2017). Delineating environmental control of phytoplankton biomass and phenology in the Southern Ocean. *Geophysical Research Letters*, *44*, 5016–5024. https://doi.org/10.1002/2016GL072428

Bakker, D. C. E., Pfeil, B., Smith, K., Harasawa, S., Landa, C., Nakaoka, S., et al. (2015). A 58-year record of high-quality data in version 3 of the Surface Ocean $CO_2$ Atlas (SOCAT). *Earth System Science Data Discuss*.

Behrenfeld, M. J. (2010). Abandoning Sverdrup's critical depth hypothesis on phytoplankton blooms. *Ecology*, *91*(4), 977–989. https://doi.org/10.1890/09-1207.1

Belcher, S. E., Grant, A. L., Hanley, K. E., Fox-Kemper, B., Van Roekel, L., Sullivan, P. P., et al. (2012). A global perspective on Langmuir turbulence in the ocean surface boundary layer. *Geophysical Research Letters*, *39*(18). https://doi.org/10.1029/2012GL052932

Blain, S., Quéguiner, B., Armand, L., Belviso, S., Bombled, B., Bopp, L., et al. (2007). Effect of natural iron fertilization on carbon sequestration in the Southern Ocean. *Nature*, *446*(7139), 1070–1074. https://doi.org/10.1038/nature05700

Blain, S., Renaut, S., Xing, X., Claustre, H., & Guinet, C. (2013). Instrumented elephant seals reveal the seasonality in chlorophyll and light-mixing regime in the iron-fertilized Southern Ocean. *Geophysical Research Letters*, *40*, 6368–6372.

Blain, S., Sarthou, G., & Laan, P. (2008). Distribution of dissolved iron during the natural iron-fertilization experiment KEOPS (Kerguelen Plateau, Southern Ocean). *Deep Sea Research Part II: Topical Studies in Oceanography*, *55*(5–7), 594–605.

Boutin, J., Merlivat, L., Hénocq, C., Martin, N., & Sallée, J. B. (2008). Air-sea $CO_2$ flux variability in frontal regions of the Southern Ocean from CARbon Interface OCean Atmosphere drifters. *Limnology and Oceanography*, *53*(5part2, 2062–2079.

Boyd, P. W., Watson, A. J., Law, C. S., Abraham, E. R., Trull, T., Murdoch, R., et al. (2000). A mesoscale phytoplankton bloom in the polar Southern Ocean stimulated by iron fertilization. *Nature*, *407*(6805), 695–702. https://doi.org/10.1038/35037500

de Boyer Montégut, C., Madec, G., Fischer, A. S., Lazar, A., & Iudicone, D. (2004). Mixed layer depth over the global ocean: An examination of profile data and a profile-based climatology. *Journal of Geophysical Research*, *109*(C12). https://doi.org/10.1029/2004JC002378

Bracegirdle, T. J., Shuckburgh, E., Sallee, J. B., Wang, Z., Meijers, A. J., Bruneau, N., et al. (2013). Assessment of surface winds over the Atlantic, Indian, and Pacific Ocean sectors of the Southern Ocean in CMIP5 models: Historical bias, forcing response, and state dependence. *Journal of Geophysical Research: Atmospheres*, *118*, 547–562. https://doi.org/10.1002/jgrd.50153

Brody, S. R., & Lozier, M. S. (2014). Changes in dominant mixing length scales as a driver of subpolar phytoplankton bloom initiation in the North Atlantic. *Geophysical Research Letters*, *41*, 3197–3203. https://doi.org/10.1002/2014GL059707

Brody, S. R., & Lozier, M. S. (2015). Characterizing upper-ocean mixing and its effect on the spring phytoplankton bloom with in situ data. *ICES Journal of Marine Science*, *72*(6), 1961–1970.

Carranza, M. M., & Gille, S. T. (2015). Southern Ocean wind-driven entrainment enhances satellite chlorophyll-a through the summer. *Journal of Geophysical Research: Oceans*, *120*, 304–323. https://doi.org/10.1002/2014JC010203

Carranza, M. M., Gille, S. T., Franks, P. J., Johnson, K. S., Pinkel, R., & Girton, J. B. (2018). When mixed layers are not mixed. Storm-driven mixing and bio-optical vertical gradients in mixed layers of the Southern Ocean. *Journal of Geophysical Research: Oceans*, *123*, 7264–7289. https://doi.org/10.1029/2018JC014416

Cassar, N., Bender, M. L., Barnett, B. A., Fan, S., Moxim, W. J., Levy, H., & Tilbrook, B. (2007). The Southern Ocean biological response to aeolian iron deposition. *Science*, *317*(5841), 1067–1070. https://doi.org/10.1126/science.1144602

Chiswell, S. M. (2011). Annual cycles and spring blooms in phytoplankton: Don't abandon Sverdrup completely. *Marine Ecology Progress Series*, *443*, 39–50.

Denman, K. L., & Gargett, A. E. (1983). Time and space scales of vertical mixing and advection of phytoplankton in the upper ocean. *Limnology and Oceanography*, *28*(5), 801–815.

Dickson, A. G., & Millero, F. J. (1987). A comparison of the equilibrium constants for the dissociation of carbonic acid in seawater media. *Deep Sea Research Part A. Oceanographic Research Papers*, *34*(10), 1733–1743.

Dong, S., Sprintall, J., Gille, S. T., & Talley, L. (2008). Southern Ocean mixed-layer depth from Argo float profiles. *Journal of Geophysical Research*, *113*(C6). https://doi.org/10.1029/2006JC004051

Gille, S. T., Carranza, M. M., Cambra, R., & Morrow, R. (2014). Wind-induced upwelling in the Kerguelen Plateau region. *Biogeosciences*, *11*(22), 6389–6400.

Gray, A. R., Johnson, K. S., Bushinsky, S. M., Riser, S. C., Russell, J. L., Talley, L. D., et al. (2018). Autonomous biogeochemical floats detect significant carbon dioxide outgassing in the high-latitude Southern Ocean. *Geophysical Research Letters*, *45*, 9049–9057. https://doi.org/10.1029/2018GL078013

Holte, J., & Talley, L. (2009). A new algorithm for finding mixed layer depths with applications to Argo data and Subantarctic Mode Water formation. *Journal of Atmospheric and Oceanic Technology*, *26*(9), 1920–1939.

Jones, J. M., Gille, S. T., Goosse, H., Abram, N. J., Canziani, P. O., Charman, D. J., et al. (2016). Assessing recent trends in high-latitude Southern Hemisphere surface climate. *Nature Climate Change*, *6*(10), 917.

Jouandet, M. P., Blain, S., Metzl, N., Brunet, C., Trull, T. W., & Obernosterer, I. (2008). A seasonal carbon budget for a naturally iron-fertilized bloom over the Kerguelen Plateau in the Southern Ocean. *Deep Sea Research Part II: Topical Studies in Oceanography*, *55*(5–7), 856–867.

Kraus, E. B., & Turner, J. S. (1967). A one-dimensional model of the seasonal thermocline II. The general theory and its consequences. *Tellus*, *19*(1), 98–106.

Lacour, L., Briggs, N., Claustre, H., Ardyna, M., & Dall'Olmo, G. (2019). The intraseasonal dynamics of the mixed layer pump in the subpolar North Atlantic Ocean: A Biogeochemical-Argo float approach. *Global Biogeochemical Cycles*, *33*(3), 266–281.

Landschützer, P., Gruber, N., Haumann, F. A., Rödenbeck, C., Bakker, D. C., Van Heuven, S., et al. (2015). The reinvigoration of the Southern Ocean carbon sink. *Science*, *349*(6253), 1221–1224. https://doi.org/10.1126/science.aab2620

Lévy, M., Franks, P. J., & Smith, K. S. (2018). The role of submesoscale currents in structuring marine ecosystems. *Nature Communications*, *9*(1), 1–16.

Mahadevan, A., D'asaro, E., Lee, C., & Perry, M. J. (2012). Eddy-driven stratification initiates North Atlantic spring phytoplankton blooms. *Science*, *337*(6090), 54–58. https://doi.org/10.1126/science.1218740

Mahadevan, A., Tandon, A., & Ferrari, R. (2010). Rapid changes in mixed layer stratification driven by submesoscale instabilities and winds. *Journal of Geophysical Research*, *115*(C3). https://doi.org/10.1029/2008JC005203

Martin, J. H. (1990). Glacial-interglacial $CO_2$ change: The iron hypothesis. *Paleoceanography*, *5*(1), 1–13.

Mehrbach, C., Culberson, C. H., Hawley, J. E., & Pytkowicx, R. M. (1973). Measurement of the apparent dissociation constants of carbonic acid in seawater at atmospheric pressure 1. *Limnology and Oceanography*, *18*(6), 897–907.

Merlivat, L., Boutin, J., & Antoine, D. (2015). Roles of biological and physical processes in driving seasonal air-sea $CO_2$ flux in the Southern Ocean: New insights from CARIOCA $pCO_2$. *Journal of Marine Systems*, *147*, 9–20.

Merlivat, L., Boutin, J., Antoine, D., Beaumont, L., Golbol, M., & Vellucci, V. (2017). Increase of dissolved inorganic carbon and decrease of pH in near surface waters of the Mediterranean Sea during the past two decades. *Biogeosciences*, *15*(18), 5653–5662.

Mignot, A., Claustre, H., Uitz, J., Poteau, A., D'Ortenzio, F., & Xing, X. (2014). Understanding the seasonal dynamics of phytoplankton biomass and the deep chlorophyll maximum in oligotrophic environments: A Bio-Argo float investigation. *Global Biogeochemical Cycles*, *28*(8), 856–876.

Mignot, A., Ferrari, R., & Claustre, H. (2018). Floats with bio-optical sensors reveal what processes trigger the North Atlantic bloom. *Nature Communications*, *9*(1), 1–9. https://doi.org/10.1038/s41467-017-02143-6

Minas, H. J., Minas, M., & Packard, T. T. (1986). Productivity in upwelling areas deduced from hydrographic and chemical fields 1. *Limnology and Oceanography*, *31*(6), 1182–1206.

Obernosterer, I., Christaki, U., Lefèvre, D., Catala, P., Van Wambeke, F., & Lebaron, P. (2008). Rapid bacterial mineralization of organic carbon produced during a phytoplankton bloom induced by natural iron fertilization in the Southern Ocean. *Deep Sea Research Part II: Topical Studies in Oceanography*, *55*(5–7), 777–789.

Park, Y. H., Fuda, J. L., Durand, I., & Garabato, A. C. N. (2008). Internal tides and vertical mixing over the Kerguelen Plateau. *Deep Sea Research Part II: Topical Studies in Oceanography*, *55*(5–7), 582–593.

Pellichero, V., Sallée, J. B., Schmidtko, S., Roquet, F., & Charrassin, J. B. (2017). The ocean mixed layer under Southern Ocean sea-ice: Seasonal cycle and forcing. *Journal of Geophysical Research: Oceans*, *122*(2), 1608–1633.

Resplandy, L., Boutin, J., & Merlivat, L. (2014). Observed small spatial scale and seasonal variability of the $CO_2$ system in the Southern Ocean. *Biogeosciences*, *11*, 75–90.

Riley, J. J., & Lelong, M. P. (2000). Fluid motions in the presence of strong stable stratification. *Annual Review of Fluid Mechanics*, *32*(1), 613–657.

Roesler, C., Uitz, J., Claustre, H., Boss, E., Xing, X., Organelli, E., et al. (2017). Recommendations for obtaining unbiased chlorophyll estimates from in situ chlorophyll fluorometers: A global analysis of WET Labs ECO sensors. *Limnology and Oceanography: Methods*, *15*(6), 572–585.

Rosso, I., Hogg, A. M., Matear, R., & Strutton, P. G. (2016). Quantifying the influence of sub-mesoscale dynamics on the supply of iron to Southern Ocean phytoplankton blooms. *Deep Sea Research Part I: Oceanographic Research Papers*, *115*, 199–209.

Sallée, J. B., Llort, J., Tagliabue, A., & Lévy, M. (2015). Characterization of distinct bloom phenology regimes in the Southern Ocean. *ICES Journal of Marine Science*, *72*(6), 1985–1998.

Sallée, J. B., Speer, K. G., & Rintoul, S. R. (2010). Zonally asymmetric response of the Southern Ocean mixed-layer depth to the Southern Annular Mode. *Nature Geoscience*, *3*(4), 273.

Sallée, J. B., Wienders, N., Speer, K., & Morrow, R. (2006). Formation of Subantarctic Mode Water in the southeastern Indian Ocean. *Ocean Dynamics*, *56*(5–6), 525–542.

Schmechtig, C., & Thierry, V. (2016). Argo quality control manual for biogeochemical data. https://doi.org/10.13155/40879.

Shadwick, E. H., Trull, T. W., Tilbrook, B., Sutton, A. J., Schulz, E., & Sabine, C. L. (2015). Seasonality of biological and physical controls on surface ocean $CO_2$ from hourly observations at the Southern Ocean Time Series site south of Australia. *Global Biogeochemical Cycles*, *29*(2), 223–238.

Siegelman, L., Klein, P., Rivière, P., Thompson, A. F., Torres, H. S., Flexas, M., & Menemenlis, D. (2020). Enhanced upward heat transport at deep submesoscale ocean fronts. *Nature Geoscience*, *13*(1), 50–55.

Stevens, C., Ward, B., Law, C., & Walkington, M. (2011). Surface layer mixing during the SAGE ocean fertilization experiment. *Deep Sea Research Part II: Topical Studies in Oceanography*, *58*(6), 776–785.

Sverdrup, H. U. (1953). On vernal blooming of phytoplankton. *Conseil Exp. Mer*, *18*, 287–295.

Taylor, J. R., & Ferrari, R. (2011). Shutdown of turbulent convection as a new criterion for the onset of spring phytoplankton blooms. *Limnology and Oceanography*, *56*(6), 2293–2307.

Thomalla, S. J., Fauchereau, N., Swart, S., & Monteiro, P. M. S. (2011). Regional scale characteristics of the seasonal cycle of chlorophyll in the Southern Ocean. *Biogeosciences*, *8*(10), 2849.

Wanninkhof, R. (2014). Relationship between wind speed and gas exchange over the ocean revisited. *Limnology and Oceanography: Methods*, *12*(6), 351–362.

Weeding, B., & Trull, T. W. (2014). Hourly oxygen and total gas tension measurements at the Southern Ocean Time Series site reveal winter ventilation and spring net community production. *Journal of Geophysical Research: Oceans*, *119*, 348–358.